JOURNAL OF GEOPHYSICAL RESEARCH, VOL. 106, NO. A10, PAGES 21,351–21,365, OCTOBER 1, 2001

Midcourse Space Experiment: Auroral enhancement of nitric oxide medium-wave infrared emission observed by the Spatial Infrared Imaging Telescope III radiometer

R. D. Sharma,[1] R. O'Neil,[1] H. Gardiner,[1] J. Gibson,[1] H. Dothe,[2]
J. W. Duff,[2] P. P. Wintersteiner,[3] and M. Kendra[4]

Abstract. Enhanced medium-wave infrared nitric oxide fundamental ($\Delta v = -1$) vibration-rotation (VR) band emission observed by the Midcourse Space Experiment radiometer band A (6.8–10.8 μm) at nighttime in the 110- to 130-km tangent altitude range on November 10, 1996, is shown to be the result of auroral dosing. The energy flux Q (ergs cm^{-2} s^{-1}), the average energy $\langle E \rangle$ (keV) of the incident electrons, as well as the location of the dosed region along the line of sight (LOS) were previously derived [*Strickland et al*., 1997]. Combining these results with the N_2^+ first negative band emission at 391.4 nm gives the auroral energy deposition rate in all three spatial dimensions. The portion of the LOS NO VR band radiance transmitted by the band A filter calculated by a more elaborate version of the auroral model in the Strategic High-Altitude Radiance Code agrees remarkably well with the enhancements in the signal observed in that band of the Spatial Infrared Imaging Telescope III radiometer.

1. Introduction

The Midcourse Space Experiment (MSX) [*Mill et al*., 1994], sponsored by the Ballistic Missile Defense Organization, was a multisensor payload designed to perform target and background measurements over a broad range from the ultraviolet to the longwave infrared (0.1–26 μm). The primary instrument for infrared observations was the Spatial Infrared Imaging Telescope III (SPIRIT III), which operated under cryogenic conditions from launch in April 1996 to the end of cryogen in February 1997 and provided simultaneous coverage in five spectral bands for a wide variety of Earth limb, terrestrial, and celestial backgrounds, including a number of limb-viewing experiments to observe the auroral region. In addition, the Ultraviolet/Visible Imaging and Spectrographic Imaging (UVISI) suite of sensors aboard MSX, coaligned with the SPIRIT III radiometer, monitored emission from N_2 (Lyman-Birge-Hopfield (LBH), 2 PG), N_2^+ 1 NG, and O I(557.7 nm) among numerous other emissions.

The MSX/SPIRIT III radiometer band A (full width at half maximum, 6.8–10.8 μm) monitored the emission from H_2O, O_3, and NO among other infrared atmospheric radiators. Above ~105 km, where the H_2O and O_3 densities are so low that their signal is below the instrument noise, the radiometer band A records primarily the nonrejected Earth radiance (NRER), a term used to describe the radiation leaking into the telescope from the warmer and denser lower atmosphere. It also detects a portion of the fundamental vibration-rotation band emission from nascent NO formed by the reaction of $N(^2D)$ and $N(^4S)$ atoms with O_2. The radiometer A filter blocks the rotationally thermalized emission around 5.3 μm from the first fundamental vibration-rotation band, i.e., [$NO(v' = 1) \rightarrow NO(v'' = 0)$] transition, populated primarily by collisions of $NO(v = 0)$ with O [*Sharma and Duff*, 1997] and secondarily from the chemically produced nascent NO. However, the filter transmits the emission from the higher fundamental bands ($v' = n \rightarrow v'' = (n - 1)$, $n > 1$) of nascent NO produced mainly by the reactions of $N(^4S)$ and $N(^2D)$ atoms with O_2 [*Sharma et al*., 1993, 1998]. Since the 5.3-μm emission from NO under quiescent nocturnal conditions in the terrestrial lower thermosphere consists primarily of the rotationally cold emission due to collisions of $NO(v = 0)$ with O [*Sharma et al*., 1996], the band A signal from quiescent nighttime conditions above ~105 km tangent altitude was dominated by nonrejected Earth radiance (NRER). However, under bright auroral dosing, the enhanced chemiluminescent emissions were recorded up to ~130 km tangent altitude. The production of N atoms is among one of the first consequences of inputting energy into the atmosphere, and nascent NO is the easiest diagnostic of the production of N atoms. Therefore the increase in the density of NO and the chemiluminescent infrared emission from nascent NO in the aurorally dosed atmosphere has been the subject of a number of recent studies [*Callis*, 1997; *Duff et al*., 1997; *Solomon et al*., 1999; *Sharma et al*., 2000]. The suggestion has been advanced that the NO in the mesosphere is transported down from the thermosphere [*Solomon et al*., 1982; *Siskind and Russell*, 1996; *Siskind et al*., 1997; *Barth et al*., 1999] to lower altitudes and latitudes where it influences the local chemistry. The local rate of production of NO and its precursors is a very important component of, and therefore of great relevance to, the models of NO in the thermosphere and mesosphere. In this article we show that the MSX radiometer band A observations during a strong auroral event permit us to model the local rate of production of NO as well as $N(^2D)$ in the lower thermosphere.

[1]Air Force Research Laboratory, Space Vehicles Directorate, Hanscom Air Force Base, Massachusetts.
[2]Spectral Sciences, Inc., Burlington, Massachusetts.
[3]ARCON Corporation, Waltham, Massachusetts.
[4]Radex Inc., Bedford, Massachusetts.

Paper number 2001JA000001.
0148-0227/01/2001JA000001$09.00

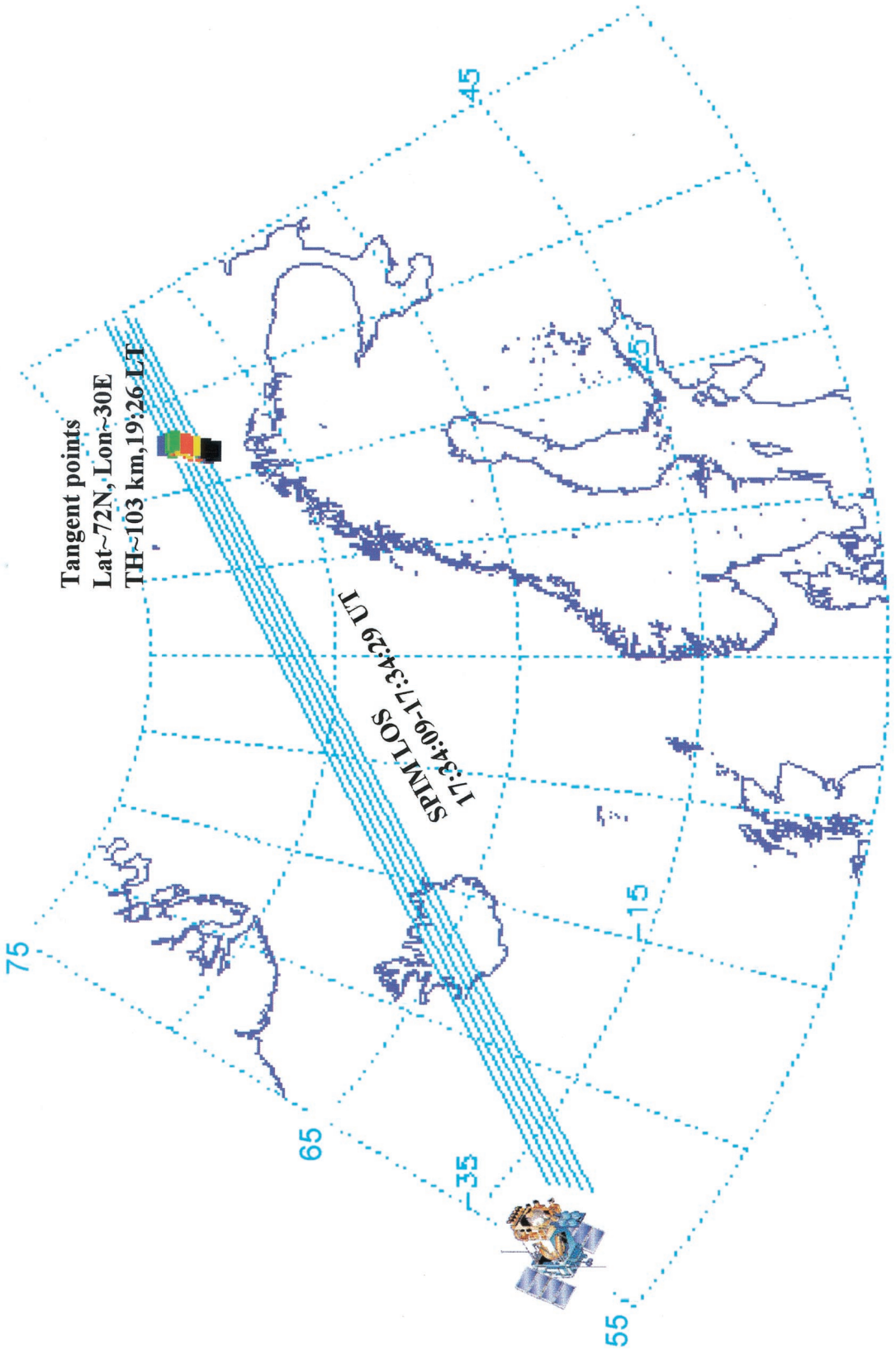

Plate 1. The Spectral Imagers (SPIMs) lines of sight every 5 s starting from the bottom at 1734:09 UT. The tangent points at 103-km altitude are located near longitude 30°E and latitude 72°N. The local time at the tangent points is ~1926. The tangent point follows the motion of the satellite and moves northeastward as shown in Figure 1.

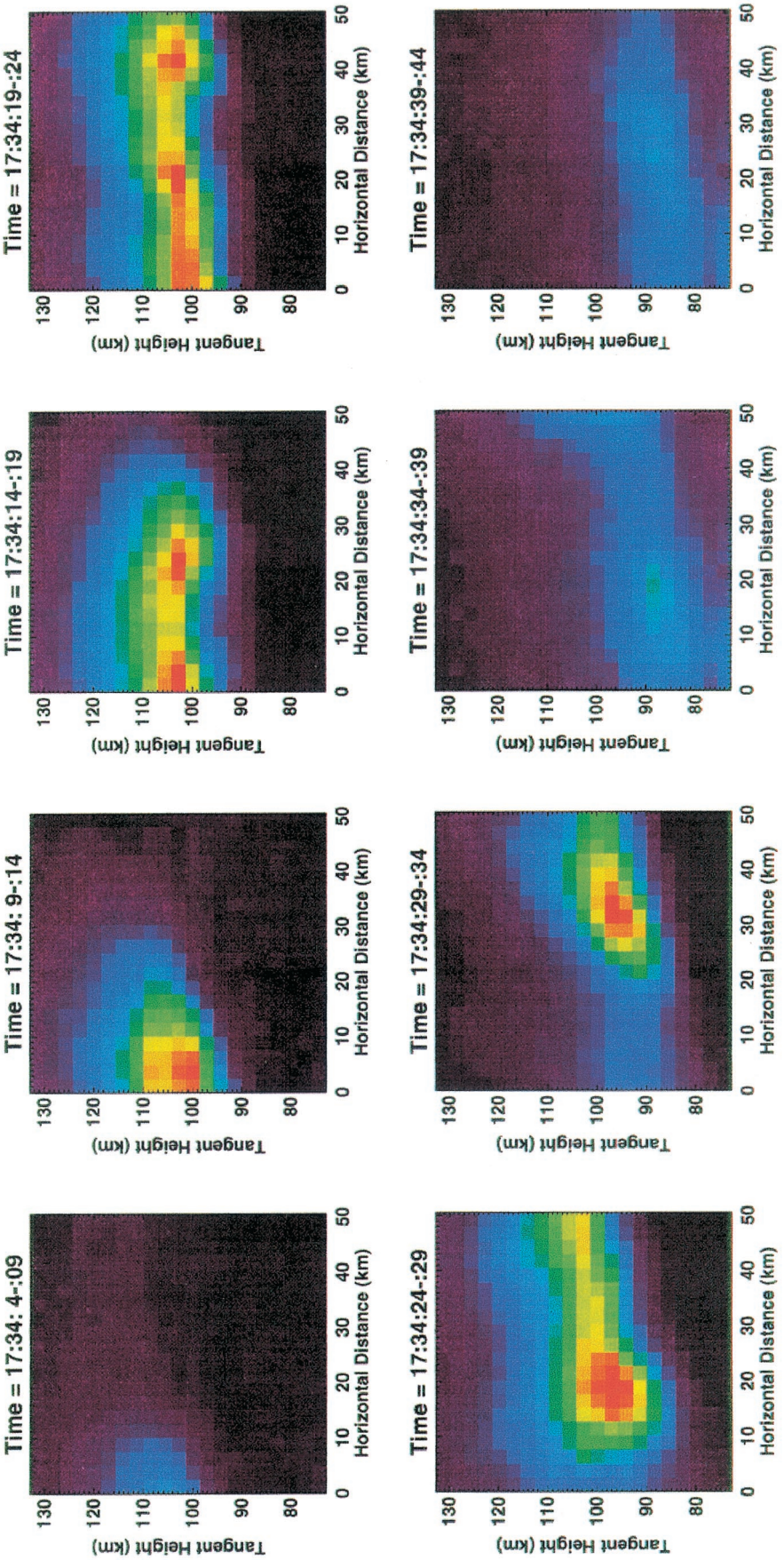

Plate 2. The 391.4-nm emission observed by SPIM 4 in the 1734:04–1734:44 UT time interval as a function of tangent altitude and horizontal distance perpendicular to the LOS from the tangent point located at 25 km in the frames. The point to note is that although this emission, and the auroral dosing causing it, moves to lower tangent altitudes and toward the tangent point, it nevertheless stays almost constant in brightness.

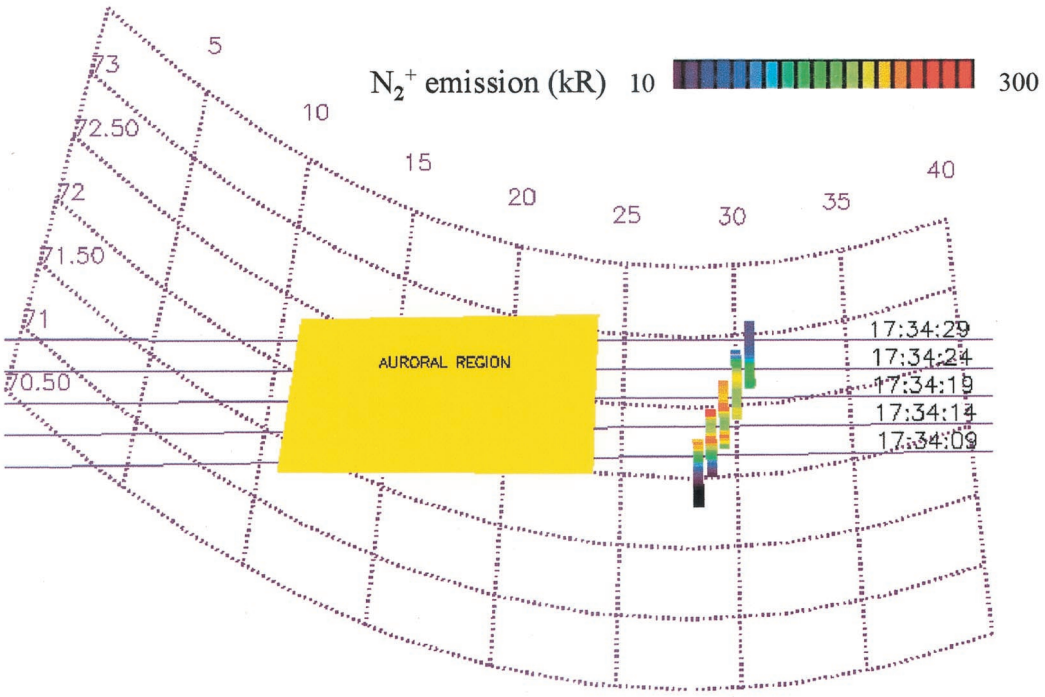

Plate 3. View from space looking down on the auroral region and lines of sight at 1734:09–1734:29 and tangent altitude 103 km. The bars show the brightness of the N_2^+ first negative emission at 391.4 nm along the horizontal, perpendicular to the LOS (HPLOS) at 103-km tangent altitude. The 391.4-nm emission shows that the auroral dosing along the HPLOS is variable. The aurorally dosed region is centered about 400 km from the tangent point toward the satellite with a bell-shape extent of 100 km half width along the LOS. The extent of the auroral region along the HPLOS is also shown in Plate 3.

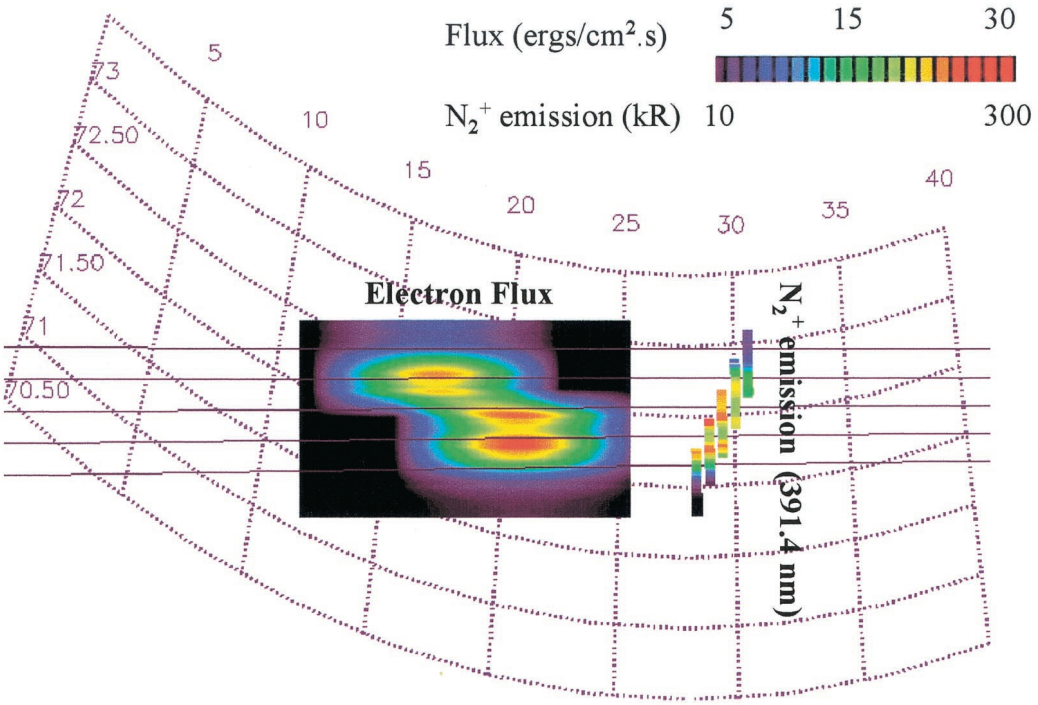

Plate 4. Location of the aurorally dosed region and the five tangent points in the geographical space. The variation of the intensity of the first negative emission from N_2^+ at 391.4 nm at the TP in the horizontal direction perpendicular to the LOS is represented by the five vertical bars, which also show, not to scale, the recession of the aurorally dosed region from the TP.

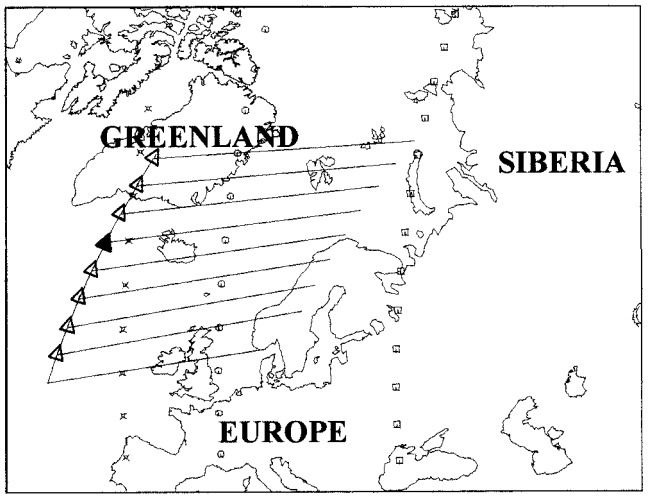

Figure 1. Minute-by-minute projection of the geographical position of the satellite (triangles) from 1730 to 1738 UT. The projections of the bore sight tangent points are at the end of the projections of the line of sight (LOS) originating from the satellite. A series of crosses, circles, and squares denote the position of the terminator at the ground, at 105-km altitude, and at the satellite altitude (900 km). The tangent points and most of the LOS are currently in the dark. The position of the terminator at 900 km, shown by squares, is still beyond the tangent point, making darkness at the tangent point a recent occurrence.

2. MSX/UVISI and SPIRIT III Radiometer Band A Observations

Among the MSX observations was a very strong auroral event observed on the night of November 10, 1996, over Scandinavia [*Strickland et al*., 1997; *Fraser et al*., 1997; *Wintersteiner et al*., 1997] around 1734 UT. Figure 1 shows a set of lines of sight (LOS) of the MSX satellite central bore sight during this time period. Plate 1 illustrates five LOS from this set, specifically from 1734:09 to 1734:29 UT in 5-s intervals, intersecting the auroral region (shown in rainbow color). The radiometer instrument consists of a vertical array of pixels, sampling the scene at 360 Hz and utilizing a mirror that sweeps, side to side, through $\pm 1.5°$ about the central bore sight every 14.3 s. Figure 2 plots the resulting locus of tangent points (TPs) traced by the radiometer central pixel, as well as the locus of TPs traced by the central bore sight. As shown in Figure 2, the former locus periodically oscillates about the latter one. As a result of this periodic oscillation, the radiometer records periodic enhancements due to an aurorally dosed region encountered by the central bore sight LOS. Such periodic enhancements are seen after 1734 UT in Figure 3, which plots the MSX radiometer band A radiance (W cm^{-2} sr^{-1}) as a function of UT after 1700 for tangent altitudes of 110 ± 0.1, 120 ± 0.1, and 130 ± 0.1 km. The radiometer mirror modulates the radiometer output and causes a dip at one extreme position (upper turning point in Figure 2) and complete loss of signal at the other extreme

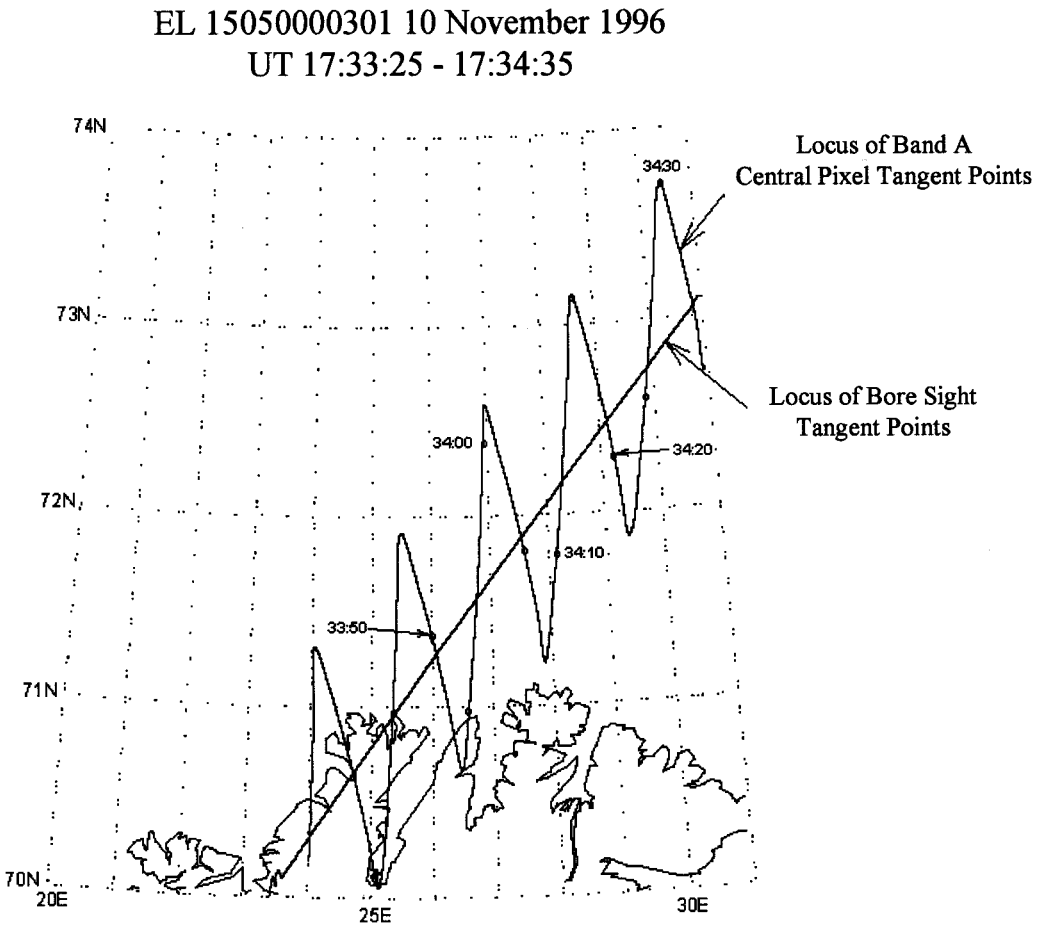

Figure 2. Projection of the locus of band A central pixel point showing mirror scan motion and the locus of the bore sight tangent points (TPs) on the geographical space.

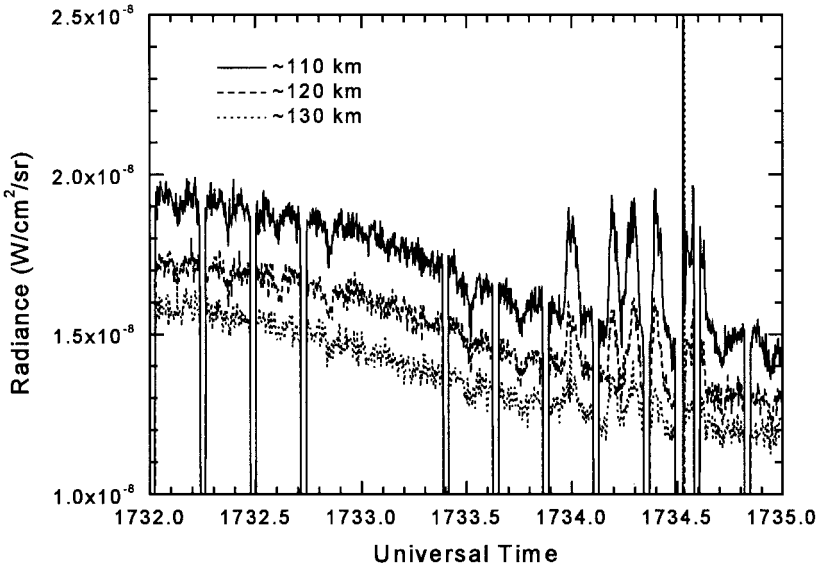

Figure 3. The radiance observed by the Midcourse Space Experiment (MSX) radiometer band A as a function of UT after 1700 for tangent altitudes of 110 (solid line), 120 (dashed line), and 130 (dotted line) km. The vertical double lines show the signal going to zero and recovering every 14.3 s at one extreme position of the mirror, and the dip in the signal halfway between these lines marks the other extreme position of the mirror. The spike in the signal shortly after 34.5 min is the instrument noise. The motion of the mirror was altogether stopped around 1733 UT for about two cycles.

position (lower turning point in Figure 2) during turnaround; the dip in the signal therefore appears at the midpoint between the loss-of-signal lines in Figure 3. In addition, the motion of the mirror was altogether stopped around 1733 UT for about two cycles. The slow decrease in the signal with time in Figure 3 after 1732:30 UT is due to the northeast motion of the satellite resulting in smaller NRER from a colder (higher latitude) and darker (greater longitude) atmosphere. Until >1734 UT the radiometer band A signal is dominated by NRER. Since the MSX/SPIRIT III radiometer band A (6.8–10.8 μm) is opaque to the first fundamental ($v = 1 \rightarrow v = 0$) NO VR band emission, owing primarily to inelastic impacts of NO($v = 0$) with O, the enhanced emissions that are detected for ~0.7 min after that time can only be attributed to chemiluminescent emission from nascent NO resulting from auroral dosing; the spike shortly after 1734:5 UT is instrument noise. It is this observed enhancement that we analyze in this paper to derive the rates of production of N(^2D) and NO. The enhancements appear periodically owing to the oscillation of radiometer mirror, as mentioned above.

It should be noted that band B (B1, 4.22–4.36 μm; B2, 4.24–4.45 μm) of the radiometer, which recorded the 4.3-μm emission from CO_2, from the same region detected similar periodic enhancements in its signal during the same time period [*Winick et al*., 1997]. Data from the UVISI Spectrographic Imagers (SPIMs) were used to derive the energy and the spatial extent of the auroral energy deposition. There were five SPIMs having the same pointing and LOS, each covering a portion of the wavelength region from the FUV to the NIR. Each SPIM simultaneously recorded spectra in each of 20 spatial pixels aligned to view a horizontal region centered on the MSX bore sight. Moreover, a moving mirror caused the field of view (FOV) to scan in the vertical direction. With 20 discrete vertical positions and a frame rate of 4 Hz, each SPIM acquired a 20 × 20 pixel spectral image every 5 s, covering a field of ~60 km (tangent height) by 50 km (horizontal) near the tangent point. Portions of the spectra were integrated to isolate specific emissions. It is the SPIM horizontal motion which when combined with the analysis of *Strickland et al*. [1997] gives us the dosing profile in all three spatial dimensions. It should be noted that there was no side-to-side mirror motion for the SPIMs as there was for the radiometers. In section 3 we give a description of the procedure used to derive the spatial extent (in geographical coordinates) of the aurorally dosed region.

3. Particle Precipitation and Associated Energy Deposition

The energy flux Q (ergs cm^{-2} s^{-1}) and the average energy $\langle E \rangle$ (keV) of the incident electrons were previously derived [*Strickland et al*., 1997] from an analysis of the LBH and second positive (2 PG) band systems of N_2 observed by the UVISI SPIM suite of sensors aboard MSX on November 10, 1996. Performing a tomographic analysis, *Strickland et al*. [1997], assuming constant auroral dosing for the 5 s it took to obtain a complete altitude scan, derived a distribution along the LOS of the intensity parameter $\langle Q_0 \rangle$ and hardness parameter $\langle E_0 \rangle$ characterizing the dosing profile for the 5-s period around 1734:28 UT. The $\langle Q_0 \rangle$ distribution may be approximated by a Gaussian function, centered at a distance of ~400 km from the TP toward the satellite with an extent of ~200 km along the LOS, characterized by $\langle Q_{\max} \rangle = 30$ ergs cm^{-2} s^{-1} and a constant $\langle E_0 \rangle = 8$ keV. The key to characterizing the LOS distribution of the electron energy flux is wavelength-dependent opacity effects due to O_2 absorption that were seen in the recorded LBH emission. The N_2^+ first negative emissions observed concurrently by the SPIM 4 sensor are shown in Plate 2 as a series of contiguous 5-s scans of images of tangent height (TH) range from ~75 to 130 km and 50-km horizontal distance

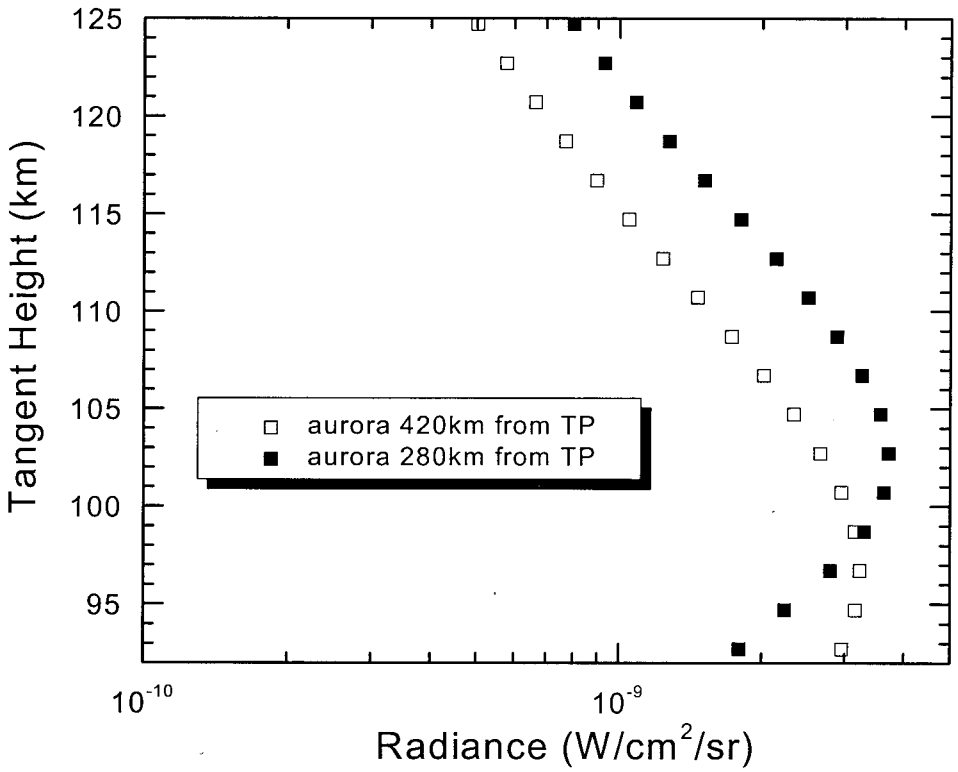

Figure 4. Effect of distance of the aurorally dosed region from the tangent on the LOS radiance. Open squares are for modeled radiance when the auroral region (peak value at tangent altitude 98 km) is 420 km from the TP while solid squares are for modeled radiance when the auroral region (peak value at tangent altitude 103 km) is 280 km from the TP. The strength of auroral dosing is the same in both cases. The ratio of the two radiances is constant for LOS with tangent altitudes greater than 103 km.

centered about the bore sight TP. Plate 2 shows that the aurorally dosed region is roughly stable in the 1734:09–1734:34 UT interval. The apparent drift of the structure is caused by the satellite motion, indicated in Figure 1. In Plate 3 the frames corresponding to 103-km TH at the TP and perpendicular to the LOS are plotted for the five contiguous 5-s SPIM scans starting at 1734:09 UT and ending at 1734:34 UT. The stability of the dosed region is supported by the geographical (latitude/longitude) coincidence of the tangent points with the most intense emission in each of the five frames. Five LOS, at 9, 14, 19, 24, and 29 s after 1734 UT, are also shown in Plate 3 defining four 5-s time blocks. Based on the result of *Strickland et al*. [1997], the aurorally dosed region can be loosely represented by the yellow rectangular area with a 200-km extent and centered at 400 km from the TP, as shown in Plate 3. However, a more detailed definition using the derived dosing profile of Strickland et al. is only possible for the region corresponding to the last 5-s time block. Additional information is required to describe the structure of the entire dosed region, as discussed below.

It should be noted in Plate 2 that the most intense emissions appear to come from $TH \approx 103$ km for the two earlier scans of SPIM data starting at 1734:09 UT and from $TH \approx 98$ km for the two later ones starting at 1734:24 UT. This behavior can be explained as the effect on the LOS radiance of the changing distances of the aurorally dosed region from the tangent point. Figure 4 plots the calculated LOS radiance as a function of tangent altitude for two auroral regions described by Gaussian dosing profiles centered at distances of 280 and 420 km from the tangent point. It is noted that the closer (farther) the auroral region is to the tangent point, the higher (lower) the apparent TH of the LOS emission. From this information the aurorally dosed region is derived as shown in Plate 4. Because *Strickland et al*. [1997] used an average over a 5-s period to derive the dosing profile shown in Plate 2 a scaling procedure for $\langle Q_{\max} \rangle$, based on the intensity of N_2^+ 391.4-nm signal, is assumed to describe the variations within the 5-s block. The dosing along the LOS shown in Plate 4 is a Gaussian profile centered at 280 km from the TP, for the early two 5-s blocks (defined by the five LOS shown), and at 420 km from the TP for the later two 5-s blocks. The decreased intensity of the N_2^+ 391.4-nm signal in the horizontal direction perpendicular to the last two LOS seen in Plate 4, in spite of the fact that the auroral dosing stays constant, is due to the motion of the dosed region away from the TP. The five TPs of the five LOS shown span the geographical space between 72°–73° latitude and 28°–31° longitude. The variation of the intensity of the auroral dosing across the LOS is obtained by scaling $\langle Q_{\max} \rangle$ with the intensity of the N_2^+ 391.4-nm signal.

4. Auroral Model

The density of nitric oxide is known to be significantly enhanced during auroral activity [*Winick et al*., 1987; *Siskind et al*., 1989; *Solomon et al*., 1999]. The impacts of the incident (primary) and secondary electrons with the ambient atmosphere cause ionization and dissociation, producing, among other species, nitrogen atoms in the ground $N(^4S)$ and excited $N(^2D)$

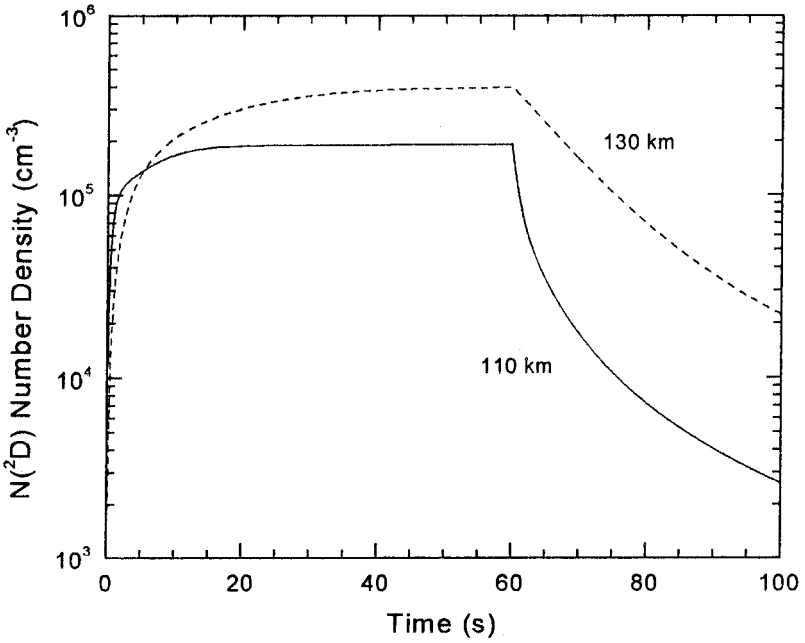

Figure 5. Rise and decay of N(^2D) density with auroral dosing at 110- and 130-km altitude. The auroral dosing at the MSX level is turned on at $t = 0$ s and turned off at $t = 60$ s.

and N(^2P) states. From the derived dosing parameters as a function of geographic coordinates, the primary electron energy deposition is calculated for segments along the SPIRIT III radiometer LOS by using the semi-empirical model of *Rees* [1963]. This model has also been used in numerous other studies of auroral emission [*Rees and Jones*, 1973; *Rees and Romick*, 1985; *Winick et al*., 1987]. The present calculations are performed with an improved research version of the Strategic High-Altitude Radiance Code (SHARC) [*Sundberg et al*., 1995]. The improved research version of the SHARC model solves ~17,000 time- and energy-dependent rate equations to calculate the energy distribution of the secondary electrons and their subsequent interaction with the ambient atmosphere. The total ion pair production rate is obtained using the procedure described by *Rees and Jones* [1973].

The present model of auroral enhancement of NO employs a time-dependent chemical kinetics model for the formation and quenching of N(^4S) atoms as well as their reaction with O_2. The importance of translationally "hot" N(^4S) atoms is quantitatively assessed by solving a time-dependent Boltzmann equation using realistic potential functions taking into account the energy and angular dependence of the sources and thermalizing sinks of these atoms [*Dothe et al*., 1997; *Sharma et al*., 1998]. The SHARC auroral chemistry code uses N(^4S) + O_2 quasi-classical trajectory reaction cross sections [*Duff et al*., 1994] to compute the rates of production of vibrationally and rotationally excited NO. The vibrational distribution of NO resulting from the N(^2D) + O_2 reaction is taken from *Winick et al*. [1987]. Although the superexcited rotational distribution of NO produced by the N(^4S) + O_2 reaction is not assumed to be relaxed, the rotational distribution of NO produced by the N(^2D) + O_2 reaction in the lower thermosphere, in accord with the observations of the Field-Widened Interferometer Rocket Experiment [*Picard et al*., 1987], is assumed to be thermal. The rate of production of NO by the N(^2P) + O_2 reaction [*Rawlins et al*., 1989] was calculated to be smaller at all altitudes than that due to the N(^2D) + O_2 reaction but more important than the N(^4S) + O_2 reaction at lower altitudes (~110 km).

The model atmosphere used was the one obtained from the empirical SHARC atmospheric generator [*Alder-Golden*, 1993] using the geomagnetic conditions appropriate to the MSX observations. Our auroral model showed that the N(^2D) density attained a steady state (rate of production equals rate of loss) at 110-km altitude in less than 1 s after the start of dosing into a quiescent atmosphere (Figure 5) while the time required for the nonthermal energetic N(^4S) atoms to reach steady state is even shorter [*Dothe et al*., 1997]. In addition, the time required for chemiluminescent NO to radiatively decay is considerably less than 1 s (radiative decay time for $1 \rightarrow 0$ vibrational transition $\approx$ 0.08 s). Less than 1 s therefore elapses between the creation of an N(^2D) atom and the appearance of a 5.3-μm photon from NO formed by its destruction by O_2. The observed 5.3-μm emission may therefore be considered "prompt"; its calculation does not require the auroral dosing time history.

Figures 6a and 6b are plots of the calculated volume emission from nascent NO produced by the reactions of N(^2D) and N(^4S) atoms with O_2 as a function of the frequency at altitudes of 110 and 130 km, respectively. It is seen from Figures 6a and 6b that the fundamental vibration-rotation band chemiluminescence near 5.3 μm (1875 cm^{-1}) due to the reaction of N(^4S) atoms is smaller than that due to the reaction of N(^2D) atoms by ~2 orders of magnitude at 110-km altitude and by a factor of at least 20 at 130-km altitude. Contribution of N(^4S) atoms to the chemical production of NO may therefore be neglected even at 130-km altitude. This is in contrast to the daytime situation where both reactions make comparable contributions to the 5.3-μm chemiluminescence at 130-km altitude [*Sharma et al*., 1998].

Table 1 gives the principal sources of N(^2D) atoms and NO molecules produced after the establishment of a steady state, a few seconds after the onset of auroral dosing, at 110- and 130-km altitudes. The number of N(^2D) atoms created per ion

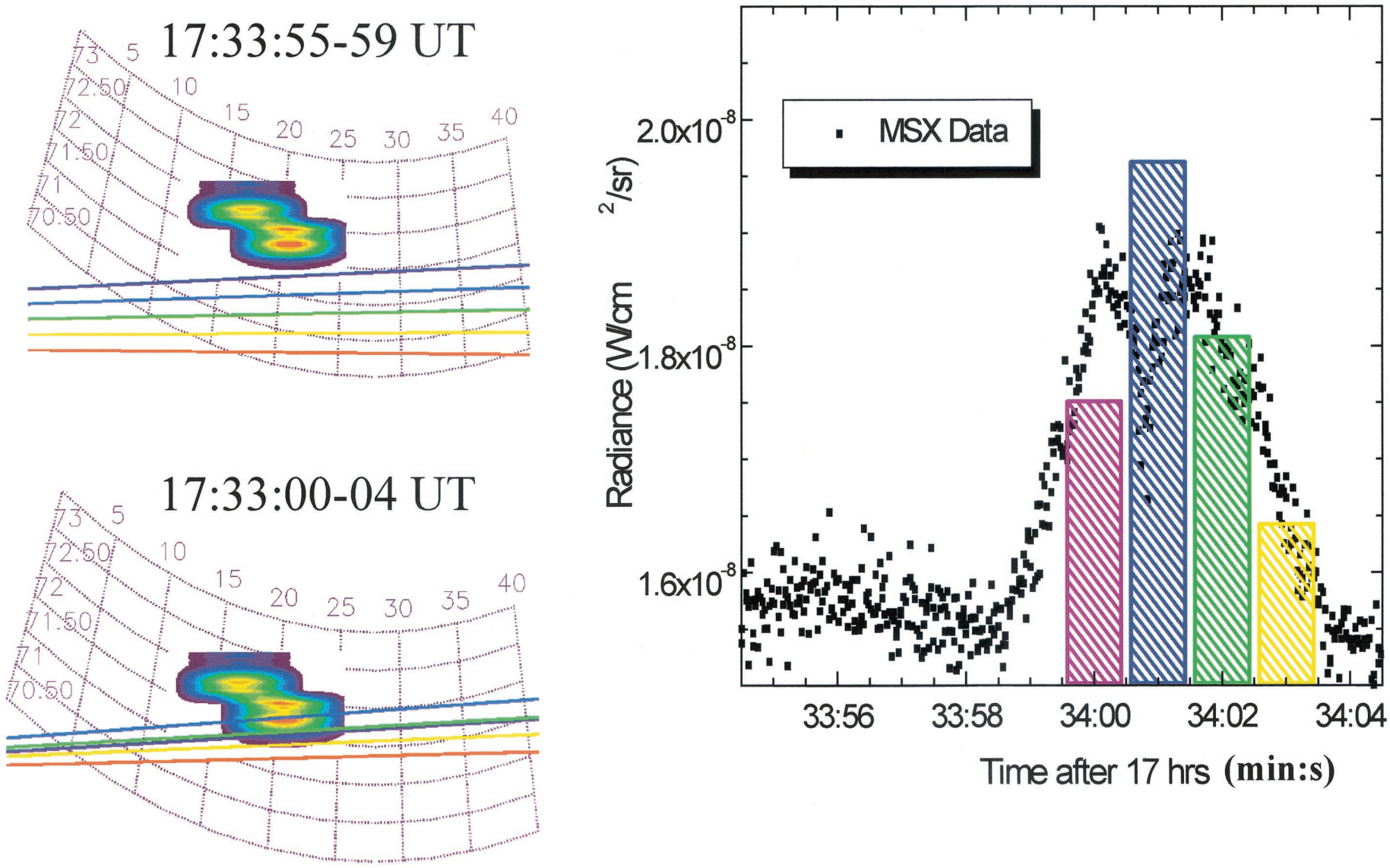

Plate 5. Aurorally dosed region and SPIRIT III LOS for *TH* = 110-km altitude for 1733:55–1733:04 UT and measured (points) and calculated (histograms with 1-s resolution) radiance. The LOS does not intersect the auroral region for 1733:55–1733:59 and 1734:04 UT. The LOS and calculated radiance for the same 1-s period have the same color. The dip in the measured radiance near 1734:01 UT is due to the motion of the mirror.

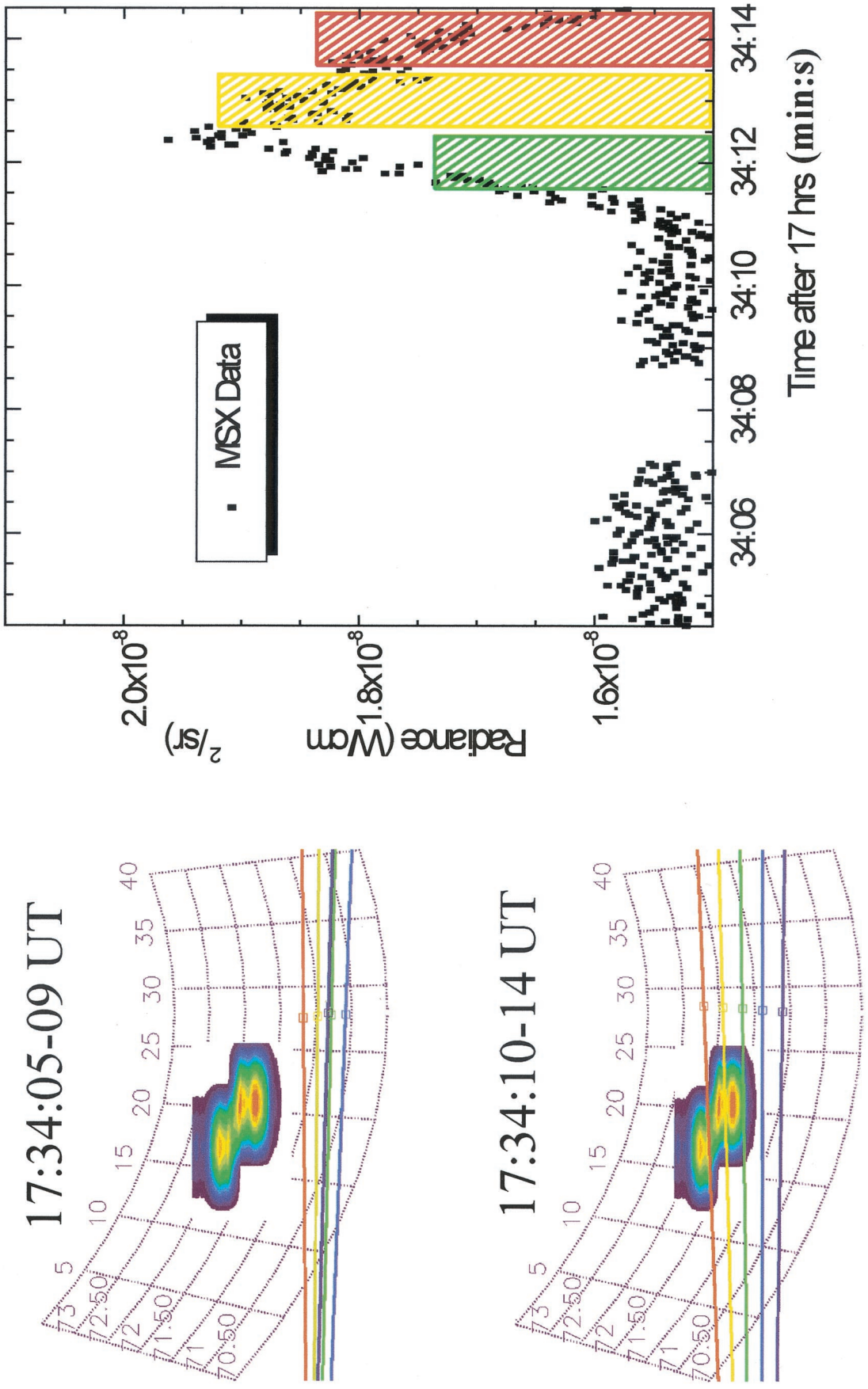

Plate 6. Aurorally dosed region and SPIRIT III LOS for TH = 110-km altitude for 1734:05–1734:14 UT and measured and calculated radiance. Loss of signal near 1734:08 UT is due to the motion of the mirror.

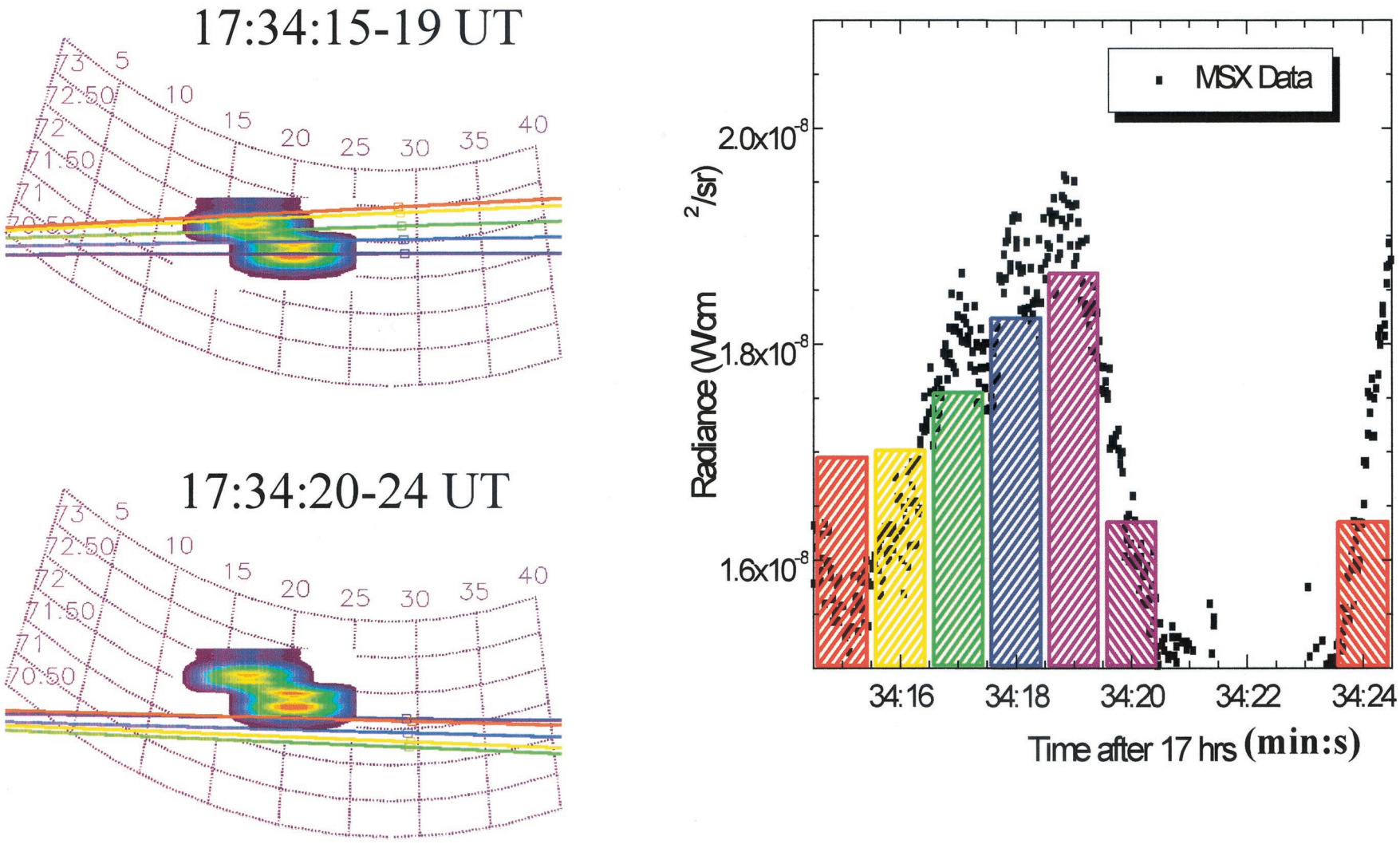

Plate 7. Aurorally dosed region and SPIRIT III LOS for TH = 110-km altitude for 1734:15–1734:24 UT and measured and calculated radiance. Dip and complete loss of signal near 1734:15 and 1734:22 UT, respectively, are due to the motion of the mirror.

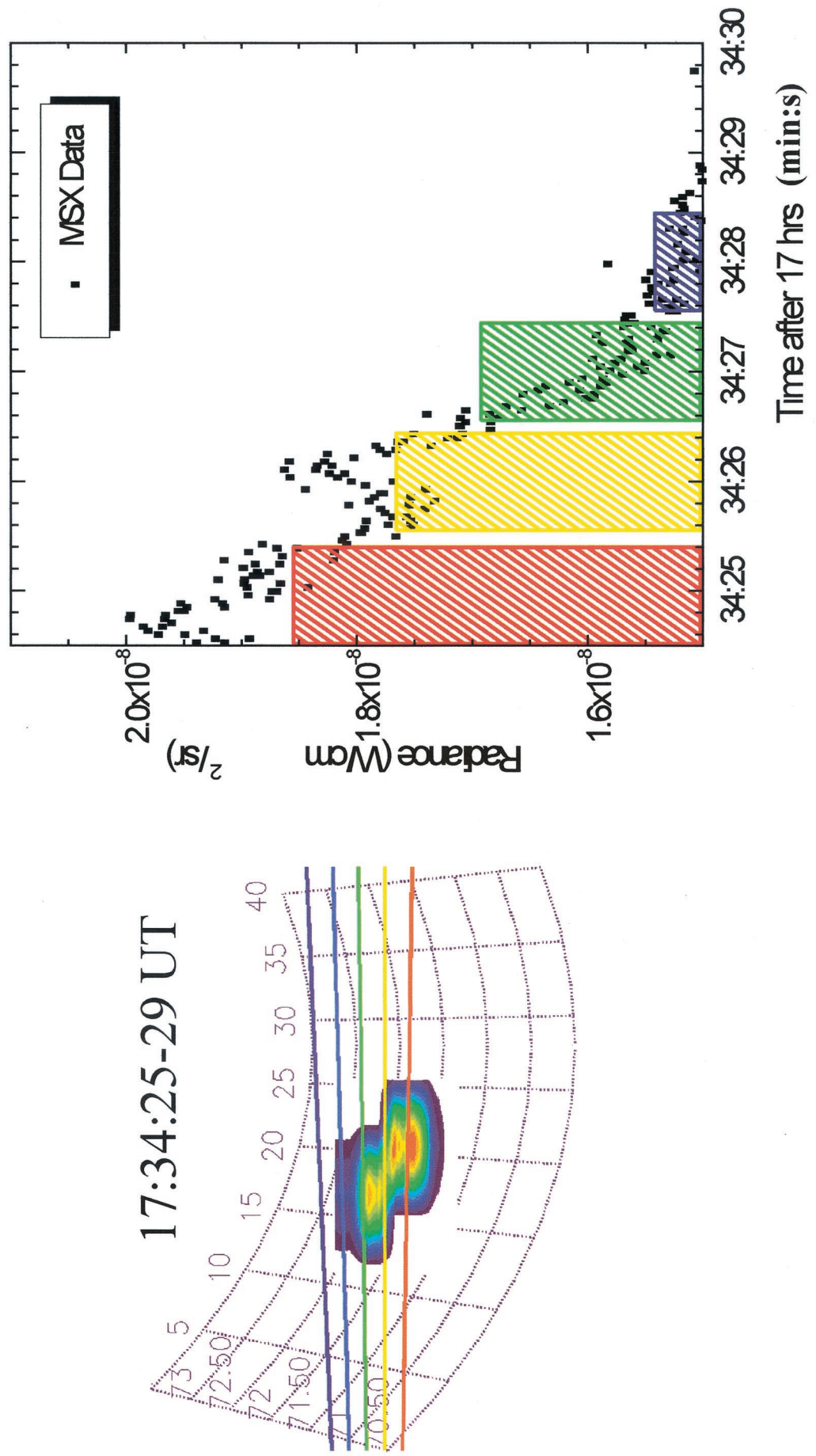

Plate 8. Aurorally dosed region and SPIRIT III LOS for $TH = 110$-km altitude for 1734:25–1734:29 UT and measured and calculated radiance. The LOS does not intersect the dosed region at 1734:29 UT.

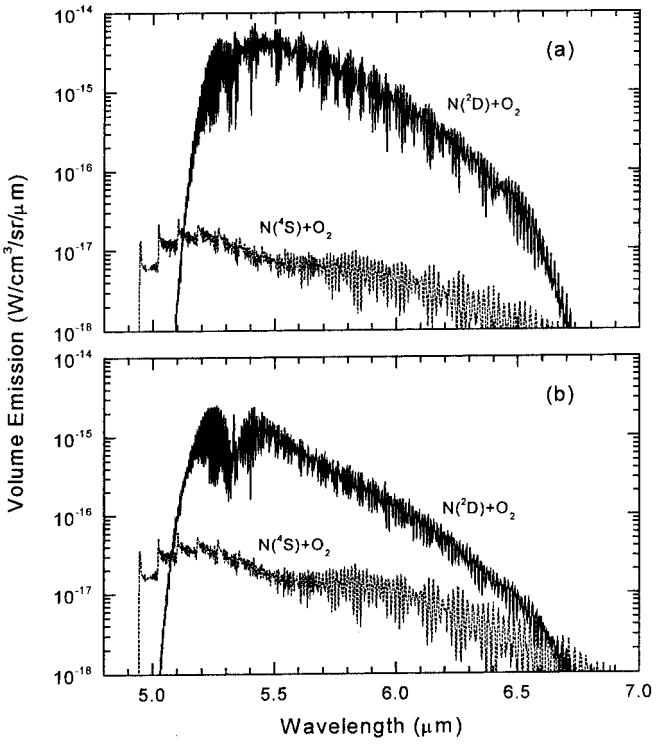

Figure 6. Spectrally resolved volume rate of fundamental vibration-rotation band emission by chemiluminescent NO produced by the reaction of $N(^4S)$ and $N(^2D)$ with O_2 at (a) 110-km altitude and (b) 130-km altitude.

pair is 1.68 and 1.92 at 110- and 130-km altitudes, respectively. Since it takes ~35 eV to create an ion pair [*Winick et al.*, 1987], the energy needed to create one $N(^2D)$ atom in the lower thermosphere is ~20 eV. This is a useful number that can be used to estimate the number of these atoms produced by auroral dosing in the lower thermosphere. Table 1 also gives the contribution of various reactions toward the production of NO and shows that the $N(^2D) + O_2$ reaction is its dominant source. In contrast to the daylit atmosphere where the reaction of $N(^4S)$ atoms with O_2 begins to overtake the $N(^2D) + O_2$ reaction as the dominant source of NO, the latter reaction produces NO at 130-km altitude at a rate which is ~15 times faster than that produced by the former reaction. The number of NO molecules formed per ion pair shows that almost all the $N(^2D)$ atoms formed at 110 km react with O_2 to form NO whereas at 130-km altitude about one third of these atoms are lost, mostly through deactivation by collisions with O atoms.

Figures 7a and 7b plot the calculated LOS radiance at 130-km tangent altitude from vibrationally excited $NO(v = 1)$ produced by the inelastic impacts of $NO(v = 0)$ with atomic oxygen and from nascent $NO(v)$ produced by the reactions of N atoms with O_2, respectively, as a function of frequency. Also shown in Figures 7a and 7b is the MSX band A filter transmittance curve. It is seen that the transmitted portion of the emission produced by the collisions of NO and O is negligible compared to the chemiluminescent emission transmitted by the filter. At lower altitudes where the chemiluminescent emission increases because of higher density (Figures 6a and 6b) while that produced by the inelastic impacts decreases, because of the lower ambient temperature, this ratio is expected to be even larger. Therefore the emission detected by the MSX band A filter may be considered solely due to nascent NO produced by the reaction of $N(^2D)$ atoms with O_2.

5. Comparison of the Calculated Radiances With the MSX Observations

Plates 5–8 give a detailed comparison of the model results with the data. On the right, Plates 5–8 show the enhancement, above the background NRER level, of the band A radiometer data for a tangent height of 110 km as a function of time, and they superimpose it with bars representing second-by-second model results calculated for the band A filter according to the description given above. The good quantitative agreement of the model calculation with the measured enhancement of emission indicates that the model accounts for the principal physical processes responsible for the auroral emission detected in this band. On the left-hand side of each of Plates 5–8 the LOS are overlaid on the auroral dosing region, also on a second-by-second basis. It is noted that the shown LOS are

Table 1. Rates of Production of $N(^2D)$ and NO[a]

	Production Rate, $cm^{-3}\ s^{-1}$	
	110-km Altitude	130-km Altitude
$e_p + N_2 \rightarrow e_p + N(^4S) + N(^2D)$	3.41×10^4	7.48×10^3
$e_p + N_2 \rightarrow e_s + ep + N^+ + N(^2D)$	1.09×10^4	2.39×10^3
$e_s + N_2 \rightarrow e_s + N(^4S) + N(^2D)$	1.93×10^4	4.15×10^3
$e + N_2^+ \rightarrow N(^4S) + N(^2D)$	5.63×10^2	5.34×10^2
$e + NO^+ \rightarrow O + N(^2D)$	1.13×10^5	2.74×10^4
$e_s + N(^2P) \rightarrow e_s + N(^2D)$	2.31×10^2	9.70×10^1
$N_2^+ + O \rightarrow NO^+ + N(^2D)$	6.34×10^4	1.93×10^4
Total $N(^2D)$	2.41×10^5	6.14×10^4
Total ion pair	1.44×10^5	3.19×10^4
NO by $N(^2D) + O_2$ reaction	2.41×10^5	3.60×10^4
NO by $N(^2P) + O_2$ reaction	7.0×10^3	0.4×10^3
NO by hot $N(^4S) + O_2$ reaction	1.4×10^3	2.5×10^3
NO by $N_2(A) + O$ reaction	1.04×10^4	0.18×10^4
Total NO	2.60×10^5	4.07×10^4

[a] The primary, secondary, and total ambient electrons are denoted by e_p, e_s, and e, respectively. The number of $N(^2D)$ atoms produced per ion pair is 1.68 and 1.92 at 110- and 130-km altitudes, respectively. The number of NO molecules produced per ion pair is 1.80 and 1.28 at 110- and 130-km altitudes, respectively. Production of NO by the $O_2^+ + N_2$ reaction was found negligible.

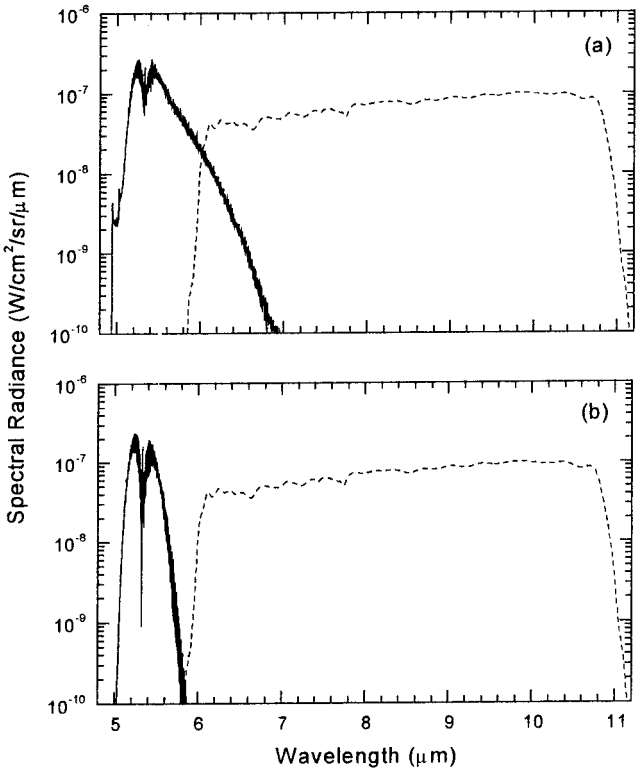

Figure 7. Spectrally resolved LOS rate of fundamental vibration-rotation band emission by NO at 130-km tangent altitude and band A filter: (a) emission from chemiluminescent NO and (b) emission from vibrational excited NO produced by the impacts of ambient NO($v = 0$) with atomic oxygen. Radiation transmitted by the filter for the case in Figure 7a is ~7 times larger than that for the case in Figure 7b.

color coded such that the colors match those of the bars representing the second-by-second model radiances. These plots show how the mirror sweeps the FOV rapidly through the region where the emissions originate. The correlation of the times of peak emission (both modeled and measured) with the LOS passing through the regions where the dosing was strongest (as determined from the 391.4-nm emission, e.g., Plate 2, and shown in false color here) provides an illustration of and additional qualitative support for the conclusion stated above. Figure 8 summarizes these results by giving a single plot of the measured auroral enhancement of the LOS emission observed by the band A radiometer and the SHARC model calculation as a function of UT after 1700.

6. Conclusion

It has been shown that the signal recorded by MSX radiometer band A during this auroral event is almost entirely due to the chemiluminescent emission from the nascent NO formed by the reaction of N(^2D) with O_2. The observed periodic enhancements in the signal observed by the MSX band A of the SPIRIT III radiometer have been shown to arise from the scan of the SPIRIT III LOS across the dosed region. Combining the energy flux Q (ergs cm^{-3} s^{-1}), the average energy $\langle E \rangle$ (keV) of the incident electrons, as well as the location of the dosed region along the LOS previously derived [*Strickland et al.*, 1997] with the N_2^+ first negative band emission at 391.4 nm observed by the Spectrographic Imager (SPIM) sensor, the auroral energy deposition rate is obtained in all three spatial dimensions. The calculated local rates of production of N(^2D) for maximum dosing are 2.41×10^5 and 6.14×10^4 cm^{-3} s^{-1} at 110- and 130-km altitude, respectively. A rough estimate of the rate of production of N(^2D) in the lower thermosphere is obtained by assuming that it takes ~20 eV of deposited auroral energy to produce one N(^2D) atom. Because of the short chemical lifetime of N(^2D) (<1 s) at 110-km altitude, the production of N(^2D) and NO by auroral dosing may be considered instantaneous; time history of auroral dosing is not required in calculating the kinetic processes involving odd N. The time dependence, observed by the MSX satellite, of the fundamental vibration-rotation band radiance from higher vibrational levels ($v \geq 2$) of NO produced mainly by the reaction of N(^2D) with O_2 is calculated with 1-s resolution. Excellent agreement between the calculated and measured radiance shows that the SHARC auroral model accurately calculates the rates of production and loss of N(^2D) and NO, the two most important odd nitrogen species.

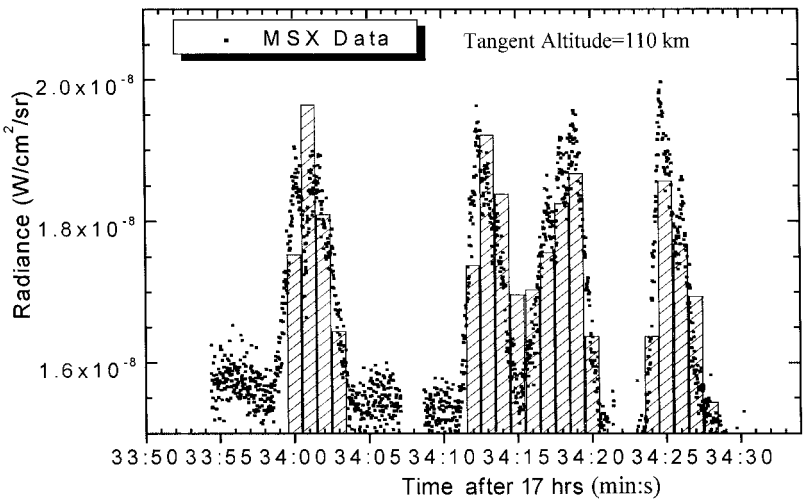

Figure 8. LOS radiance modeled (Strategic High-Altitude Radiance Code (SHARC) model) and measured (by MSX band A radiometer) as a function of 1733:50–1734:30 UT.

Acknowledgments. This research has been supported in part by AFOSR under Project 2303ES, task 92VS04COR, and in part by BMDO under Program Management Agreement PMA F3352, task 4, natural backgrounds. The MSX project was funded by BMDO. The authors are grateful to D. Strickland for providing the results of the dosing calculations and many discussions about auroral dosing.

Janet G. Luhmann thanks David E. Siskind and another referee for their assistance in evaluating this paper.

References

Alder-Golden, S., Description of the SHARC atmospheric generator, *Tech. Rep. PL-TR-93-2123*, Phillips Lab., Hanscom Air Force Base, Mass., 1993.

Barth, C. A., S. M. Bailey, and S. C. Solomon, Solar-terrestrial coupling: Solar soft x-rays and thermospheric nitric oxide, *Geophys. Res. Lett*., *26*, 1251, 1999.

Callis, L. B., Odd nitrogen formed by energetic electron precipitation as calculated from TIROS data, *Geophys. Res. Lett*., *24*, 3237, 1997.

Dothe, H., R. D. Sharma, and J. W. Duff, On the steady-state assumption for the energy distribution function of the nonthermal $N(^4S)$ atoms and the efficiency of NO production by these atoms in the terrestrial thermosphere, *Geophys. Res. Lett*., *24*, 3233, 1997.

Duff, J. W., F. Bien, and D. E. Paulsen, Classical dynamics of the $N(^4S) + O_2 \rightarrow NO(X^2\Pi) + O(^3P)$ reaction, *Geophys. Res. Lett*., *21*, 3043, 1994.

Duff, J. W., H. Dothe, and R. D. Sharma, A model for the 5.3 μm emission from NO observed by CIRRIS 1A in the aurorally dosed nighttime terrestrial thermosphere, *Eos Trans. AGU*, *78*(46), Fall Meet. Suppl., F504, 1997.

Fraser, M., W. Gallery, T. Opar, G. Romick, M. Kendra, R. Hegblom, H. Gardiner, and R. O'Neil, MSX: The aurora of 10 November 1996 observed over Scandinavia, *Eos Trans. AGU*, *78*(17), Spring Meet. Suppl., S232, 1997.

Mill, J. D., R. R. O'Neil, S. Price, G. J. Romick, O. M. Uy, E. M. Gaposchkin, G. C. Light, W. W. Moore Jr., T. L. Murdock, and A. T. Stair Jr., Midcourse Space Experiment: Introduction to the spacecraft, instruments, and scientific objectives, *J. Spacecr. Rockets*, *31*, 900, 1994.

Picard, R. H., J. R. Winick, R. D. Sharma, A. S. Zachor, P. J. Espy, and C. R. Harris, Interpretation of infrared measurements of the high-latitude thermosphere from a rocketborne interferometer, *Adv. Space Res*., *7*(10), 23, 1987.

Rawlins, W. T., M. E. Fraser, and S. M. Miller, Rovibrational excitation of nitric oxide in the reaction of O_2 with metastable atomic atomic nitrogen, *J. Chem. Phys*., *42*, 1097, 1989.

Rees, M. H., Auroral ionization and excitation by incident energetic electrons, *Planet. Space Sci*., *11*, 1209, 1963.

Rees, M. H., and R. A. Jones, Time dependent studies of the aurora-II spectroscopic morphology, *Planet. Space Sci*., *11*, 1213, 1973.

Rees, M. H., and G. J. Romick, Atomic nitrogen in aurora: Production, chemistry, and optical emissions, *J. Geophys. Res*., *90*, 9871, 1985.

Sharma, R. D., and J. W. Duff, Determination of the translational temperature of the high altitude terrestrial thermosphere from the rotational distribution of the 5.3 μm emission from $NO(v = 1)$, *Geophys. Res. Lett*., *24*, 2407, 1997.

Sharma, R. D., Y. Sun, and A. Dalgarno, Highly rotationally excited nitric oxide in the terrestrial thermosphere, *Geophys. Res. Lett*., *20*, 2043, 1993.

Sharma, R. D., V. A. Kharchenko, Y. Sun, and A. Dalgarno, Energy distribution of fast nitrogen atoms in the nighttime terrestrial thermosphere, *J. Geophys. Res*., *101*, 275, 1996.

Sharma, R. D., H. Dothe, and J. W. Duff, Model of the 5.3 μm radiance from NO during the daylit terrestrial thermosphere, *J. Geophys. Res*., *103*, 14,753, 1998.

Sharma, R. D., N. B. Wheeler, J. O. Wise, H. Dothe, and J. W. Duff, Global variation in the 2.7 μm NO overtone emission from the lower thermosphere, *Geophys. Res. Lett*., *27*, 349, 2000.

Siskind, D. E., and J. M. Russell III, Coupling between middle and upper atmospheric NO: Constraints from HALOE observations, *Geophys. Res. Lett*., *23*, 137, 1996.

Siskind, D. E., C. A. Barth, D. S. Evans, and R. G. Roble, The response of thermospheric nitric oxide to an auroral storm, 1, Auroral latitudes, *J. Geophys. Res*., *94*, 16,899, 1989.

Siskind, D. E., J. T. Bacmeister, M. E. Summers, and J. M. Russell III, Two-dimensional model calculations of nitric oxide transport in the middle atmosphere and comparison with Halogen Occultation Experiment data, *J. Geophys. Res*., *102*, 3527, 1997.

Solomon, S., P. J. Crutzen, and R. G. Roble, Photochemical coupling between the thermosphere and the lower atmosphere, 1, Odd nitrogen from 50 to 120 km, *J. Geophys. Res*., *87*, 7206, 1982.

Solomon, S. C., C. A. Barth, and S. M. Bailey, Auroral production of nitric oxide measured by the SNOE satellite, *Geophys. Res. Lett*., *26*, 1259, 1999.

Strickland, D. J., T. Majeed, J. Bishop, R. J. Cox, J. S. Evans, G. J. Romick, M. D. Morrison, D. E. Anderson, L. J. Paxton, and C. I. Meng, Characterization of particle precipitation and associated energy deposition for an auroral event on 10 November 1996 based on MSX UVISI imaging and spectral radiance data, *Eos Trans. AGU*, *78*(17), Spring Meet. Suppl., S232, 1997.

Sundberg, R. L., J. W. Duff, J. H. Gruninger, L. S. Bernstein, M. W. Matthew, S. M. Adler-Golden, D. C. Robertson, R. D. Sharma, J. H. Brown, and R. J. Healey, SHARC: A model for calculating atmospheric infrared radiation under non-equilibrium conditions, in *The Upper Mesosphere and Lower Thermosphere: A Review of Experiment and Theory*, *Geophys. Monogr. Ser*., vol. 87, pp. 287–295, AGU, Washington, D. C., 1995.

Winick, J. R., R. H. Picard, R. A. Joseph, R. D. Sharma, and P. P. Wintersteiner, An infrared spectral radiance code for the auroral thermosphere (AARC), *AFGL-TR-87-0034*, Air Force Geophys. Lab., Hanscom Air Force Base, Mass., 1987.

Winick, J. R., R. O'Neil, H. Gardiner, J. Gibson, R. H. Picard, P. P. Wintersteiner, and M. Kendra, MSX: Analysis of strong auroral enhancement at 4.3 μm observed by the SPIRIT III radiometer, *Eos Trans. AGU*, *78*(17), Spring Meet. Suppl., S233, 1997.

Wintersteiner, P., M. Kendra, D. Strickland, G. Romick, D. Morrison, R. O'Neil, H. Gardiner, W. Gallery, and M. Fraser, MSX: Auroral visible and ultraviolet emissions, *Eos Trans. AGU*, *78*(17), Spring Meet. Suppl., S232, 1997.

H. Dothe and J. W. Duff, Spectral Sciences, Inc., 99 South Bedford Street, Burlington, MA 01803-5169.

H. Gardiner, J. Gibson, R. O'Neil, and R. D. Sharma, Air Force Research Laboratory, Space Vehicles Directorate, 29 Randolph Rd., Hanscom AFB, MA 01731-3010. (Ramesh.Sharma@hanscom.af.mil)

M. Kendra, Radex Inc., 3 Preston Court, Bedford, MA 01730.

P. P. Wintersteiner, ARCON Corporation, 260 Bear Hill Road, Waltham, MA 02154.

(Received January 2, 2001; revised February 27, 2001;
accepted February 27, 2001.)